

Transient and Steady-State Temperature Rise in Three-Dimensional Anisotropic Layered Structures in Pump-Probe Thermoreflectance Experiments

Puqing Jiang,^{1,2,a)} and Heng Ban^{1,2,b)}

¹*Department of Mechanical Engineering and Materials Science, University of Pittsburgh, Pittsburgh, Pennsylvania 15261, USA*

²*Pittsburgh Quantum Institute, Pittsburgh, Pennsylvania 15260, USA*

Abstract

Recent developments of the pump-probe thermoreflectance methods (such as the beam-offset and elliptical-beam approaches of the time-domain and frequency-domain thermoreflectance techniques) enabled measurements of the thermal conductivities of in-plane anisotropic materials. Estimating the temperature rise of anisotropic layered structures under surface heating is critically important to make sure that the temperature rise is not too high to alias the signals in these experiments. However, a simple formula to estimate the temperature rise in three-dimensional (3D) anisotropic layered systems heated by a non-circular laser beam is not available yet, which is the main problem we aim to solve in this work. We first derived general formalisms of the temperature rise for a multilayered structure by solving the 3D anisotropic heat diffusion equation in the frequency domain. These general formalisms normally require laborious numerical evaluation; however, they could be reduced to explicit analytical expressions for the case of semi-infinite solids. We then extend the analytical expressions to multilayered systems, taking into account the effect of the top layers. This work not only enhances our understanding of the physics of temperature rise due to surface laser heating but also enables quick estimation of the peak temperature rise of 3D anisotropic layered systems in pump-probe thermoreflectance experiments and thus greatly benefits the

^a puqing.jiang@pitt.edu

^b heng.ban@pitt.edu

thermoreflectance experiments in choosing the appropriate heating power and heater size for the experiments.

1. Introduction

Thermal conductivity of anisotropic materials is a critical property that impacts their wide applications in modern devices such as microelectronics,¹ photonics,² solar cells,³ thermal barrier coatings⁴, and thermoelectric modules.⁵ Accurate measurements of the three-dimensional (3D) thermal conductivity of thin films and small-scale samples were made possible with the recent development of transient techniques including the thermoreflectance methods (time-domain/frequency-domain thermoreflectance, TDTR/FDTR) and the 3ω method. These techniques have been extensively used to measure the 3D thermal conductivity tensor of both thin films and bulk materials over a wide range of thermal conductivity.^{6, 7 8-21}

The thermoreflectance methods, including both TDTR and FDTR, use a modulated pump laser beam to heat the sample and a second probe beam to detect the surface temperature change via the linear change of the surface reflectance R_s with temperature, $\Delta R_s = \frac{dR_s}{dT} \Delta T$. TDTR typically uses ultrafast pulsed lasers (with pulse widths <0.5 ps) and FDTR typically uses continuous-wave (cw) lasers for the measurements. In both cases, the surface temperature rise ΔT should not be too high to invalidate the assumption of the linear temperature dependence of R_s . Besides, since both methods measure the thermal properties of the sample at the base temperature T_0 , the surface temperature rise ΔT should not be too high to invalidate the assumption of constant thermal properties within the temperature range of T_0 to $T_0 + \Delta T$. This is particularly important at low temperatures where the heat capacities have the T^3 temperature dependence. A general guideline is that the steady-state surface temperature rise ΔT should not exceed 10 K or 10% of the absolute temperature, whichever is smaller.^{6, 22} A quick and accurate estimation of the temperature rise in both TDTR and FDTR

is thus critically important in choosing an appropriate heating power and heater size for the experiments.

For the steady-state temperature rise in thermoreflectance experiments, Cahill²³ was the first to derive an analytical expression for an isotropic semi-infinite solid, which was later extended to a more general form by Braun *et al.*²⁴ as

$$\Delta T = \frac{P_0}{\sqrt{2\pi k_z k_r (w_0^2 + w_1^2)}}. \quad (1)$$

Here, P_0 is the averaged laser power absorbed by the sample, k_r and k_z are the in-plane and through-plane thermal conductivities of the material, w_0 and w_1 are the $1/e^2$ radii of the pump and probe laser spots, and ΔT is the temperature rise as averaged by the probe beam. While Eq. (1) has been commonly used in both TDTR and FDTR experiments to estimate the steady-state temperature rise, it is limited to axially symmetric cases. Besides, the case of pulsed laser heating should be more complicated than Eq. (1). Also, as pointed out by Braun *et al.*²⁴, the layers and interfaces in multilayered systems could redistribute the heat flux and result in a temperature rise that is different from the one predicted using Eq. (1). A more general formula of the temperature rise for both cw and pulsed laser heating that can apply to multilayered systems with 3D anisotropy is urgently needed.

In this work, general formalisms of the peak temperature rise were first derived for both cw and pulsed laser heating of 3D anisotropic multilayered systems. These general formalisms were then reduced to simple semiempirical correlations to enable fast and accurate estimation of the peak temperature rise in both FDTR and TDTR experiments. These simple analytical expressions were tested against the general formalisms for several different representative cases and the effect of thin-film layers on the peak temperature rise was discussed.

2. General formalism

The heat diffusion process in anisotropic media is governed by the following equation:

$$C \frac{\partial T}{\partial t} = k_x \frac{\partial^2 T}{\partial x^2} + k_y \frac{\partial^2 T}{\partial y^2} + k_z \frac{\partial^2 T}{\partial z^2} + 2k_{xy} \frac{\partial^2 T}{\partial x \partial y} + 2k_{xz} \frac{\partial^2 T}{\partial x \partial z} + 2k_{yz} \frac{\partial^2 T}{\partial y \partial z} \quad (2)$$

Here C is the volumetric heat capacity, and $k_x, k_y, k_z, k_{xy}, k_{yz}, k_{xz}$ are the 6 independent components of the 2nd rank thermal conductivity tensor, which must be symmetric due to the constraints by the classical continuum mechanics.^{25, 26} The temperature dependence of the thermophysical properties is ignored for the sake of simplicity. This parabolic partial differential equation could be simplified to a one-dimensional (1D) heat conduction problem in the frequency domain by doing Fourier transforms to the in-plane coordinates and time, $T(x, y, z, t) \leftrightarrow \Theta(u, v, z, \omega)$. The surface temperature rise Θ_s of a multilayered system could be solved in the frequency domain as

$$\Theta_s(u, v, \omega) = \hat{G}(u, v, \omega) Q_s(u, v, \omega), \quad (3)$$

where $\hat{G}(u, v, \omega)$ is the Green's function and $Q_s(u, v, \omega)$ is the surface heat flux in the frequency domain. Details on the derivation of the Green's function can be found in [Supplementary Information Section S1](#) and also Refs. [^{10, 14}].

For the case of cw laser heating in FDTR, the surface heat flux is

$$q^{cw}(x, y, t) = \frac{2}{\pi w_x w_y} \exp \left[-2 \left(\frac{x^2}{w_x^2} + \frac{y^2}{w_y^2} \right) \right] \left[P_0 + P_1 \cos(\omega_0 t + \varphi_0) \right], \quad (4)$$

Here w_x and w_y are the $1/e^2$ radii of the pump laser spot in the x and y directions, respectively; P_0 and P_1 are the amplitudes of the offset component and the periodic heating power [in Watts] absorbed by the sample, with $P_0 \geq P_1$; ω_0 is the modulation frequency, and φ_0 is an arbitrary phase shift. Fourier transform of Eq. (4) gives its frequency-domain expression as

$$Q_s^{cw}(u, v, \omega) = 2\pi \exp\left(-\frac{\pi^2 u^2 \sigma_{x_0}^2}{2}\right) \exp\left(-\frac{\pi^2 v^2 \sigma_{y_0}^2}{2}\right) \times \left[P_0 \delta(\omega) + P_1 \frac{\delta(\omega - \omega_0) e^{i\varphi_0} + \delta(\omega + \omega_0) e^{-i\varphi_0}}{2} \right] \quad (5)$$

The case of pulsed laser heating in TDTR would be a little more complicated, with the surface heat flux expressed as

$$q^{pulsed}(x, y, t) = \frac{2}{\pi w_x w_y} \exp\left[-2\left(\frac{x^2}{w_x^2} + \frac{y^2}{w_y^2}\right)\right] \left[P_0 + P_1 \cos(\omega_0 t + \varphi_0) \right] \times \left[\frac{0.94}{f_{rep} \tau_p} \sum_{n=-\infty}^{\infty} \exp\left(-2.77 \frac{(t - nT_s - t_0)^2}{\tau_p^2}\right) \right] \quad (6)$$

This is a train of pulses with Gaussian distribution in time and space, modulated by a sinusoidal function at frequency ω_0 . The laser pulses have a full duration at half maximum (FDHM) of τ_p . The laser repetition rate is f_{rep} with a period of $T_s = 1/f_{rep}$, and t_0 is an arbitrary time shift of laser pulses. Similarly, the frequency-domain surface heat flux for the case of pulse laser heating could be obtained from the Fourier transform of Eq. (6) as:

$$Q_s^{pulsed}(u, v, \omega) = 2\pi \exp\left(-\frac{\pi^2 u^2 w_x^2}{2}\right) \exp\left(-\frac{\pi^2 v^2 w_y^2}{2}\right) \times \sum_{n=-\infty}^{\infty} \left\{ \left[P_0 \delta(\omega - n\omega_s) + P_1 \frac{\delta(\omega - n\omega_s - \omega_0) e^{i\varphi_0} + \delta(\omega - n\omega_s + \omega_0) e^{-i\varphi_0}}{2} \right] e^{\frac{n^2 \omega_s^2 \tau_p^2}{11.08}} e^{-in\omega_s t_0} \right\} \quad (7)$$

The surface temperature rise of the layered structure can thus be obtained by doing an inverse 2D Fourier transform of Eq. (3) as

$$\theta(x, y, t) = \frac{1}{2\pi} \int_{-\infty}^{\infty} \int_{-\infty}^{\infty} \int_{-\infty}^{\infty} Q_s(u, v, \omega) \hat{G}(u, v, \omega) \exp(i2\pi(ux + vy) + i\omega t) dudvd\omega \quad (8)$$

For the case of cw laser heating, the time-varying surface temperature rise is

$$\begin{aligned} \theta(x, y, t) = & P_0 \int_{-\infty}^{\infty} \int_{-\infty}^{\infty} \hat{G}(u, v, 0) \exp\left(-\frac{\pi^2 u^2 w_x^2}{2}\right) \exp\left(-\frac{\pi^2 v^2 w_y^2}{2}\right) \exp(i2\pi(ux + vy)) dudv \\ & + P_1 \int_{-\infty}^{\infty} \int_{-\infty}^{\infty} \text{Re} \left[\hat{G}(u, v, \omega_0) e^{i(\omega_0 t + \varphi_0)} \right] \exp\left(-\frac{\pi^2 u^2 w_x^2}{2}\right) \exp\left(-\frac{\pi^2 v^2 w_y^2}{2}\right) \exp(i2\pi(ux + vy)) dudv \end{aligned} \quad (9)$$

For the case of pulsed laser heating, it would be

$$\theta(x, y, t) = P_0 \sum_{n=-\infty}^{\infty} \left\{ e^{-\frac{n^2 \omega_s^2 \tau_p^2}{11.08}} e^{in\omega_s(t-t_0)} \int_{-\infty}^{\infty} \int_{-\infty}^{\infty} \hat{G}(u, v, n\omega_s) \exp\left(-\frac{\pi^2 u^2 w_x^2}{2}\right) \exp\left(-\frac{\pi^2 v^2 w_y^2}{2}\right) \exp(i2\pi(ux + vy)) dudv \right\} \\ + P_1 \sum_{n=-\infty}^{\infty} \left\{ e^{-\frac{n^2 \omega_s^2 \tau_p^2}{11.08}} e^{in\omega_s(t-t_0)} \int_{-\infty}^{\infty} \int_{-\infty}^{\infty} \text{Re} \left[\hat{G}(u, v, n\omega_s + \omega_0) e^{i\omega_0 t} \right] \exp\left(-\frac{\pi^2 u^2 w_x^2}{2}\right) \exp\left(-\frac{\pi^2 v^2 w_y^2}{2}\right) \exp(i2\pi(ux + vy)) dudv \right\} \quad (10)$$

The first terms of Eqs. (9) and (10) are the steady-state temperature rise induced by the constant offset component of the heat flux, and the second terms of Eqs. (9) and (10) are the steady periodic temperature oscillation induced by the modulated component of the surface heat flux.

Figure 1 (a, b) shows an example of the time-varying heating power of cw and pulsed laser heating with the same averaged heating power of $P_0 = 10$ mW and the same amplitude of the periodic heating power as $P_1 = 10$ mW. Here the pulsed laser has a repetition rate of $f_{\text{rep}} = 80$ MHz and a pulse width of $\tau_p = 0.5$ ps. Figure 1(b) shows that although the averaged power of the pulsed laser is only 10 mW, the instant laser power could be as high as 300 W due to the ultrashort widths of the laser pulses.

Figure 1 (c-e) shows the corresponding peak temperature rises (located at $x = y = z = 0$) of a 100 nm Al/Si two-layered system under both cw and pulsed laser heating, whose power profiles are shown in Fig. 1 (a, b). The subplots (1c-1e) are for the system at 300 K (with $k_{\text{Si}} = 140$ W/mK, $C_{\text{Si}} = 1.6$ MJ/m³K) and the subplots (2c-2e) are for the system at 70 K (with $k_{\text{Si}} = 1680$ W/mK, $C_{\text{Si}} = 0.35$ MJ/m³K). The laser spot size was fixed as $w_x = w_y = 5$ μm and the modulation frequency was chosen as 5 MHz for both cases. The blue curves in Fig. 1 are for the pulsed laser heating and the red shadowed regions represent the cw laser heating. For the time-varying temperature rise of pulsed laser heating, the data in the delay time range 0-80 ps after each pulse were omitted for the sake of clarity.

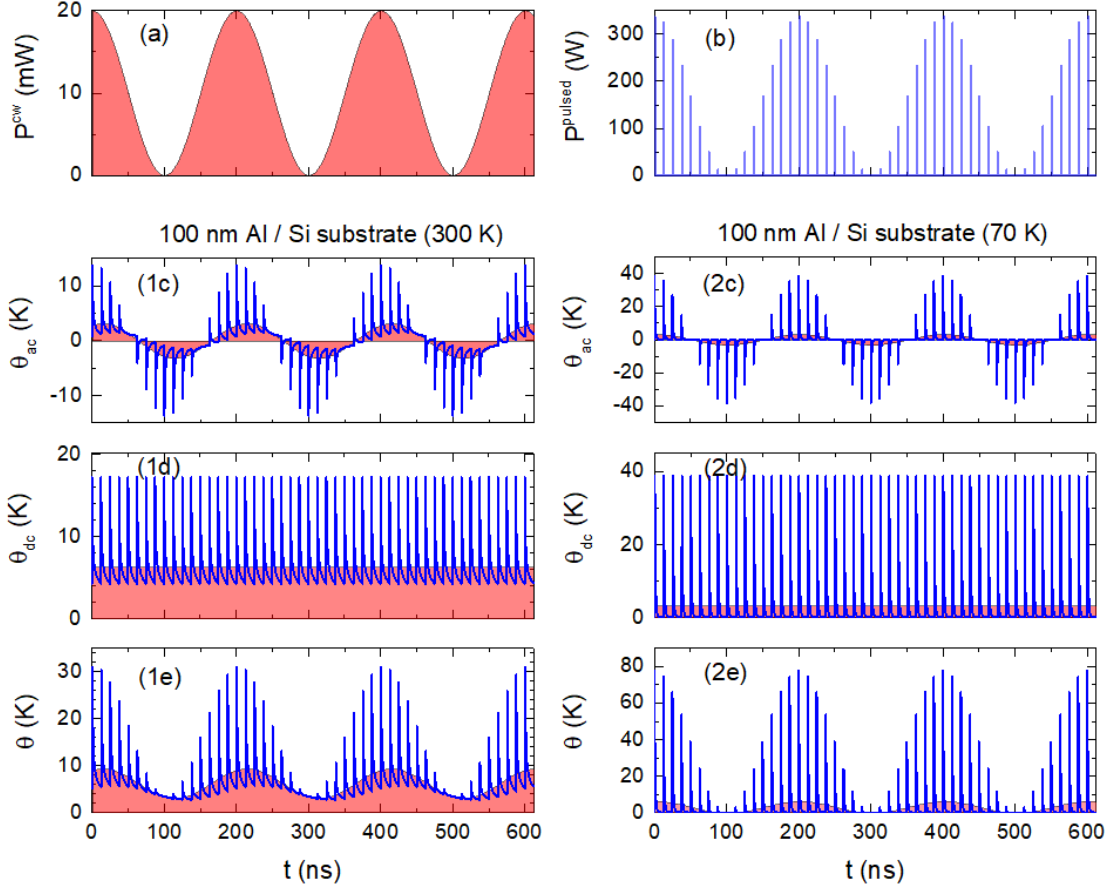


FIG. 1. (a, b) The time-varying heating power profile of modulated cw and pulsed laser with the same averaged heating power of $P_0 = 10$ mW and the same amplitude of oscillating heating power of $P_1 = 10$ mW. (c-e) The peak temperature rise (located at $x = y = z = 0$) θ_{ac} , θ_{dc} , and $\theta = \theta_{ac} + \theta_{dc}$ of a 100 nm Al/Si system as a function of time at different temperatures of 300 K (subplots 1c – 1e) and 70 K (subplots 2c – 2e) heated by both a pulsed laser (the blue curves) and a cw laser (the red shadowed region). The heating power, laser spot size, and modulation frequency are all kept the same for both cases. For the case of pulsed laser heating, the data in the delay time range 0-80 ps after each pulse were omitted for the sake of clarity.

As shown in Fig. 1 (c-e), the temperature rise of the sample consists of a steady-state component θ_{dc} induced by the constant offset component of the surface heat flux and a periodic oscillating component θ_{ac} induced by the modulated component of the surface heat flux. The amplitude of θ_{ac} is always smaller than or equal to that of θ_{dc} . For the pulsed laser

heating, the temperature rise consists of a pulse accumulation component, which has an amplitude similar to that of the cw laser heating, and a transient component induced by each pulse heating event, whose amplitude decreases approximately exponentially with the delay time after the pulse heating event. The transient component of the temperature rise at a short delay time could be much higher than that of the cw laser heating, especially at low temperatures where the sample has a high in-plane thermal diffusivity k_r/C . Therefore, it would be insufficient to only estimate the steady-state temperature rise based on Eq. (1) in TDTR experiments. In what follows, we will develop simple analytical expressions for quick estimation of the full temperature rise for both cw and pulsed laser heating. These analytical expressions also help us to identify the key parameters that affect the temperature rise and better understand the correlations among them.

3. Analytical expressions for the peak temperature rise of semi-infinite solids

The general formalisms derived above (Eqs. (9) and (10)) could be reduced to explicit analytical expressions for the simple case of a semi-infinite solid with an orthogonal thermal conductivity tensor ($k_{xy} = k_{xz} = k_{yz} = 0$), for which the Green's function is

$$\hat{G}(u, v, \omega) = \frac{1}{\sqrt{iC\omega k_z + 4\pi^2 k_z (k_x u^2 + k_y v^2)}}. \quad (11)$$

3.1 Peak temperature rise of a semi-infinite solid induced by cw laser heating

Plugging Eq. (11) into Eq. (9) and setting $x = y = 0$, the spatially peak temperature rise of a semi-infinite solid under cw laser heating is expressed as:

$$\begin{aligned} \theta^{\text{cw}} = & P_0 \int_{-\infty}^{\infty} \int_{-\infty}^{\infty} \frac{\exp(-\pi^2 u^2 w_x^2 / 2) \exp(-\pi^2 v^2 w_y^2 / 2)}{2\pi \sqrt{k_z (k_x u^2 + k_y v^2)}} dudv \\ & + P_1 \text{Re} \left[e^{i\omega t} \int_{-\infty}^{\infty} \int_{-\infty}^{\infty} \frac{\exp(-\pi^2 u^2 w_x^2 / 2) \exp(-\pi^2 v^2 w_y^2 / 2)}{\sqrt{iC\omega_0 k_z + 4\pi^2 k_z (k_x u^2 + k_y v^2)}} dudv \right]. \end{aligned} \quad (12)$$

The first term of Eq. (12), which is due to the constant offset component of the cw laser heating, can be expressed as

$$\theta_{\text{dc}}^{\text{cw}} = \frac{P_0}{\sqrt{2\pi w_0^2 k_z k_r}} \xi, \quad (13)$$

with the anisotropy correction factor $\xi\left(\frac{\alpha}{\beta}\right)$ expressed as

$$\xi\left(\frac{\alpha}{\beta}\right) = \frac{w_0}{\sqrt{2\pi}} \int_{-\infty}^{\infty} \int_{-\infty}^{\infty} \frac{\exp\left[-\pi^2 w_0^2 (u^2/\beta + \beta v^2)/2\right]}{\sqrt{(u^2/\alpha + \alpha v^2)}} dudv. \quad (14)$$

Here the anisotropy parameters are defined as $\alpha = \sqrt{k_y/k_x}$, $\beta = w_y/w_x$, and the averaged in-plane thermal conductivity and laser spot size are defined as $k_r = \sqrt{k_x k_y}$ and $w_0 = \sqrt{w_x w_y}$, respectively.

The anisotropy correction factor $\xi(\alpha/\beta)$ is a function of solely α/β and is plotted out as the solid curve in Fig. 2. It could also be approximated as $\xi(\alpha/\beta) \approx \frac{4\sqrt{\alpha\beta}}{(\sqrt{\alpha} + \sqrt{\beta})^2}$, which has an error of <2% if α/β is in the range $0.1 < \alpha/\beta < 10$ and an error of ~10% if $0.01 < \alpha/\beta < 100$, as shown by the dashed curve in Fig. 2. If the anisotropy is too large with $\alpha/\beta > 100$ or $\alpha/\beta < 0.01$, a slightly different correlation $\xi(\alpha/\beta) \approx \frac{4\left(\frac{\alpha}{\beta}\right)^{0.45}}{\left(1 + \left(\frac{\alpha}{\beta}\right)^{0.45}\right)^2}$ could be used instead to approximate ξ with an error <1%, as shown by the dash-dotted curve in Fig. 2.

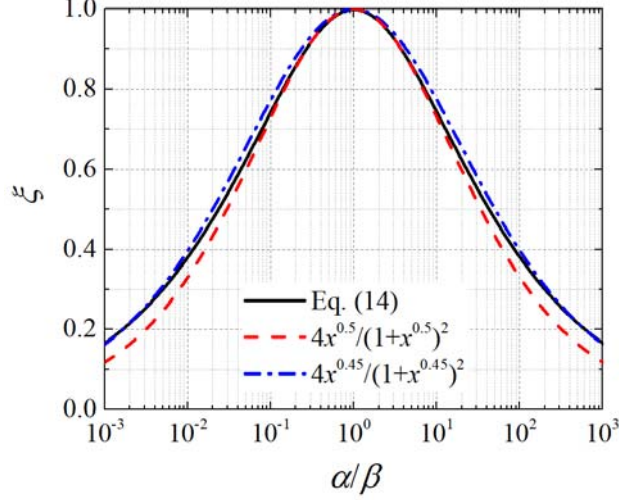


FIG. 2. The anisotropy correction factor ξ (Eq. (14)) as a function of α/β , with $\alpha = \sqrt{k_y/k_x}$ and $\beta = w_y/w_x$. The solid curve is the accurate numerical result of Eq. (14). The dashed and dash-dotted curves are the approximations.

When $\alpha = \beta$ which gives $\xi = 1$, Eq. (13) becomes identical to Eq. (1) if the probe laser spot size w_1 in Eq. (1) is set to be 0. Note that the temperature rise derived here is the peak value induced by the pump heating and is independent of the probe spot size, whereas the temperature rise derived by Cahill²³ and Braun *et al.*²⁴ was the value averaged by the Gaussian profile of the probe beam. In the limit $w_1 \rightarrow 0$, the probe beam detects only the peak temperature induced by the pump heating. In what follows, we focus only on the peak temperature rise induced by the pump beam. If in any case the probe-averaged temperature rise is desired, simply set $w_x = \sqrt{w_{x_0}^2 + w_{x_1}^2}$ and $w_y = \sqrt{w_{y_0}^2 + w_{y_1}^2}$ in the correlations, where w_{x_0} and w_{y_0} are the $1/e^2$ radii of the pump laser spot in the x and y directions, respectively, while w_{x_1} and w_{y_1} are those for the probe laser spot.

Equation (13) suggests that the steady-state temperature rise of the semi-infinite solid is proportional to both the heat flux and the square-root of the heated area, $\theta \propto \frac{q''}{k} \sqrt{A}$, where A is the heated area and $k = \sqrt{k_z k_r}$ is the averaged thermal conductivity. Therefore, even

under the continuous heating of a constant heat flux without any heat loss, a steady-state temperature rise could still be established in the semi-infinite solid if the heated area is finite. On the other hand, for the case of 1D uniform heating with an infinitely large heated area, the surface temperature rise would be $\theta = \frac{2q''}{k} \sqrt{\frac{kt}{\pi C}} \propto \sqrt{t}$, where t is the heating time,²⁷ in which case a steady state could never be established.

The second term of Eq. (12), which is due to the heating by the modulated component of the cw laser heat flux, is oscillating with time with a constant amplitude in the fully established state. To understand how the heating frequency affects the amplitude of the steady periodic temperature oscillation, we plot in Fig. 3 the ratios between the amplitudes of the periodic temperature oscillation at different heating frequencies and the steady-state temperature rise as solid curves, assuming $P_0 = P_1$. We find that the temperature rise ratios mainly depend on the normalized laser spot size $\hat{w} = w_0 / \sqrt{\frac{2\pi k_r}{\omega_0 C}}$, where w_0 and k_r are the averaged laser spot size and in-plane thermal conductivity defined as $w_0 = \sqrt{w_x w_y}$ and $k_r = \sqrt{k_x k_y}$, respectively. The amplitude of the steady periodic temperature oscillation of the semi-infinite solid is always less than or equal to its steady-state temperature rise under the same amplitude of heating power. When $w_0 \ll \sqrt{\frac{2\pi k_r}{\omega_0 C}}$ where the heat flow is highly three-dimensional, the amplitude of the periodic temperature oscillation approaches the steady-state temperature rise. On the other hand, with $w_0 \gg \sqrt{\frac{2\pi k_r}{\omega_0 C}}$ the heat flow would be one-dimensional in the z -direction; in this case, the amplitude of the periodic temperature oscillation approaches zero.

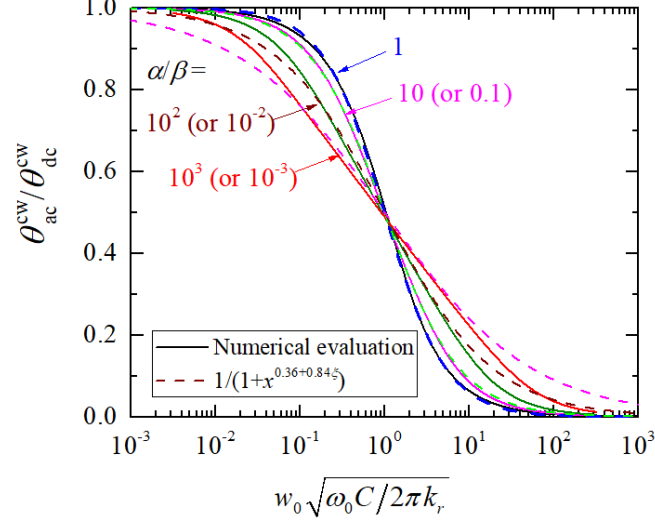


FIG. 3. The ratio of the amplitude of the periodic temperature oscillation to the steady-state temperature rise of a semi-infinite solid under the same amplitude of heating power plotted as a function of normalized laser spot size for different anisotropy ratios α/β . The solid curves are the accurate numerical results and the dashed curves are the empirical correlation predictions (Eq. (15)).

The in-plane anisotropy in both the thermal conductivity $\alpha = \sqrt{k_y/k_x}$ and laser spot size $\beta = w_y/w_x$ also affect the amplitude of periodic temperature oscillation, as shown in Fig. 3. We come up with an empirical correlation for the ratio between the amplitude of the periodic temperature oscillation at the frequency ω_0 and the steady-state temperature rise of a semi-infinite solid under cw laser heating as

$$\theta_{ac}^{cw}/\theta_{dc}^{cw} = \frac{1}{1 + \left(w_0 \sqrt{\frac{\omega_0 C}{2\pi k_r}} \right)^{0.36+0.84\xi}}. \quad (15)$$

Predictions by the correlation Eq. (15) are plotted as the dashed curves in Fig. 3 and they compare quite well with the accurate numerical results if $0.01 < \alpha/\beta < 100$.

In sum, the peak temperature rise of a semi-infinite solid under modulated cw laser heating could be estimated as

$$\theta^{\text{cw}} = \xi \frac{1}{\sqrt{2\pi w_0^2 k_z k_r}} \left\{ P_0 \pm P_1 \left[1 + \left(w_0 \sqrt{\frac{\omega_0 C}{2\pi k_r}} \right)^{0.36+0.84\xi} \right]^{-1} \right\} \quad (16)$$

The \pm sign represents the range of the temperature oscillation due to the modulated heating.

Note that the steady-state temperature rise due to cw laser heating depends only on the averaged thermal conductivity $k = \sqrt{k_z k_r}$ but not on the heat capacity of the material. Although the oscillating part of the temperature rise depends on the heat capacity, the amplitude of the oscillating part of the temperature rise is always less than or equal to the steady-state temperature rise. Therefore, the heat capacity of the material does not place a constraint on the temperature rise in FDTR experiments. The situation, however, is different in TDTR experiments, where a pulsed laser is used for the heating and the heat capacity could play an important role in the transient temperature rise, see details below.

3.2 Peak temperature rise of a semi-infinite solid induced by pulsed laser heating

Plugging Eq. (11) into Eq. (10) and setting $x = y = 0$, the spatially peak temperature rise of a semi-infinite solid under the heating of a train of modulated laser pulses is expressed as:

$$\begin{aligned} \theta^{\text{pulsed}} = & P_0 \sum_{n=-\infty}^{\infty} \left[e^{-\frac{n^2 \omega_s^2 \tau_p^2}{11.08}} e^{in\omega_s(t-t_0)} \int_{-\infty}^{\infty} \int_{-\infty}^{\infty} \frac{\exp(-\pi^2 u^2 w_x^2 / 2) \exp(-\pi^2 v^2 w_y^2 / 2)}{\sqrt{iC(n\omega_s)k_z + 4\pi^2 k_z (k_x u^2 + k_y v^2)}} dudv \right] \\ & + P_1 \text{Re} \left\{ \sum_{n=-\infty}^{\infty} \left[e^{-\frac{n^2 \omega_s^2 \tau_p^2}{11.08}} e^{in\omega_s(t-t_0)} e^{in\omega_s t} \int_{-\infty}^{\infty} \int_{-\infty}^{\infty} \frac{\exp(-\pi^2 u^2 w_x^2 / 2) \exp(-\pi^2 v^2 w_y^2 / 2)}{\sqrt{iC(\omega_0 + n\omega_s)k_z + 4\pi^2 k_z (k_x u^2 + k_y v^2)}} dudv \right] \right\}. \end{aligned} \quad (17)$$

The first term of Eq. (17) is due to the offset component of the pulsed laser heating, an example of which is shown as the blue curves in Fig. 1 (1d, 2d). This temperature rise comprises a constant component due to the pulse accumulation and a transient component due to the heating by each pulse. If the pulse repetition rate $f_{\text{rep}} \rightarrow \infty$, the pulse accumulation would approach the cw laser heating and the transient temperature rise due to each pulse would approach zero. Although Eq. (17) is hard to be reduced further analytically but

requires numerical evaluation, after analyzing the numerical results of some representative cases, we come up with the following semiempirical correlation for the first term of Eq. (17) as

$$\theta_{dc}^{\text{pulsed}} = \xi \frac{P_0}{\sqrt{2\pi w_0^2 k_z k_r}} \left[1 + \left(16 \frac{k_r}{\pi w_0^2 C} \frac{1}{f_{rep}} \right)^{0.18+0.42\xi} \right]^{-1} + \frac{1.1P_0}{f_{rep} \pi w_0^2 \sqrt{k_z C t_d}} \left(1 + \frac{25}{\xi^2} \frac{k_r}{\pi w_0^2 C} t_d \right)^{-1} \quad (18)$$

Here t_d is the time after each pulse heating event.

The first term of Eq. (18) is the pulse accumulation $\theta_{dc,accum}^{\text{pulsed}}$ and the second term is the transient component $\theta_{dc,trans}^{\text{pulsed}}$ due to the individual pulse heating events. The empirical correlation Eq. (18) has been tested against 1000 randomly chosen cases, with k_x, k_y, k_z independently and randomly varying in the range of 0.5-5000 W/mK, C varying in the range of 0.001-10 MJ/m³K, and w_x, w_y independently and randomly varying in the range of 1-100 μm . The tested anisotropy k_z/k_r and α/β have covered a wide range from 10^{-4} to 10^4 . This correlation was found to be accurate with an error of <3% for $t_d = 10$ ps if the dimensionless factor $\xi w_0 \sqrt{C f_{rep}/k_r} > 1$, which could be met in most cases in TDTR experiments. If $\xi w_0 \sqrt{C f_{rep}/k_r} < 1$ or if t_d is too large (e.g., $t_d > 1$ ns) so that the three-dimensional heat flow dominates, the simple expression of Eq. (18) would cause a larger error but still generally <50% in estimating the temperature rise due to the pulsed heating, see [Supplementary Information Section S2](#) for more details on the validation of this correlation.

From Eq. (18), we can see that the steady-state temperature rise due to pulse accumulation mainly depends on $\frac{q''}{k} \sqrt{A}$, and the transient temperature rise mainly depends on $\frac{q''}{e_z \sqrt{t_d}}$ in the short t_d range, where $e_z = \sqrt{k_z C}$ is the through-plane thermal effusivity. The ratio $w_0/\sqrt{k_r/C}$ is the key factor that determines the relative magnitudes of the steady-state temperature rise and the transient temperature rise: with $w_0 \gg \sqrt{k_r/C}$ the pulse accumulation

would dominate over the transient pulse temperature rise; on the other hand, if $w_0 \ll \sqrt{k_r/C}$, the transient pulse temperature rise could be much higher than the steady-state pulse accumulation. Therefore, only estimating the steady-state temperature rise would be insufficient in TDTR experiments especially when measuring materials with high in-plane thermal diffusivities k_r/C , an example of which is shown in Fig. 1 (2d).

The second term of Eq. (17) is more complicated since the modulation frequency ω_0 is non-zero. For the modulated pulsed laser heating, the temperature rise $\theta_{ac}^{\text{pulsed}}$ also contains a pulse accumulation component $\theta_{ac,accum}^{\text{pulsed}}$ and a transient component due to the pulse heating event $\theta_{ac,trans}^{\text{pulsed}}$, both periodically varying with time, an example of which is shown as the blue curves in Fig. 1 (1c, 2c). After analyzing the numerical results of 7000 randomly chosen cases with the modulation frequency varying in the range 10 Hz – 10 MHz, we recommend the following empirical correlations to estimate the amplitudes of $\theta_{ac}^{\text{pulsed}}$:

$$\begin{aligned} \theta_{ac}^{\text{pulsed}} = & \frac{P_1}{P_0} \theta_{dc,accum}^{\text{pulsed}} \left[1 + 4 \left(\frac{w_0}{5} \sqrt{\frac{\omega_0 C}{2\pi k_r}} \right)^{0.36+0.84\xi} \right]^{-1} \left[1 + \pi \sqrt{\frac{\omega_0}{2\pi f_{rep}}} \right]^{-1} \\ & + \frac{P_1}{P_0} \theta_{dc,trans}^{\text{pulsed}} \left[1 - \left(1 + \frac{(\omega_0/2\pi)^{-0.11\log_{10}(4t_d f_{rep})}}{-\log_{10}(4t_d f_{rep})} \right)^{-1} \left(1 + 150 \left(10w_0 \sqrt{\frac{\omega_0 C}{2\pi k_r}} \right)^{-0.6-1.4\xi} \right)^{-1} \right] \end{aligned} \quad (19)$$

The temperature oscillating range by the pulsed heating could thus be estimated as $\theta^{\text{pulsed}} = \theta_{dc}^{\text{pulsed}} \pm \theta_{ac}^{\text{pulsed}}$. The validity of Eq. (19) has been tested against the 7000 random cases, see more details in [Supplementary Information Section S3](#).

As a demonstration, we used the analytical expressions Eqs. (16, 18, 19) to estimate the peak temperature rise of a Si semi-infinite substrate heated at 300 K and 70 K and compare them in Fig. 4 with the accurate numerical evaluations. The laser power was assumed to be absorbed on the surface of the Si substrate. For the pulsed heating, the temperature rise was evaluated at a delay time t_d of 80 ps. All the other conditions are the same as those for Fig. 1.

The shadowed regions in Fig. 4 represent the estimations using the analytical expressions and the curves are the numerical evaluations. The excellent agreement between the analytical estimations and accurate numerical evaluations proves the validity of these analytical expressions.

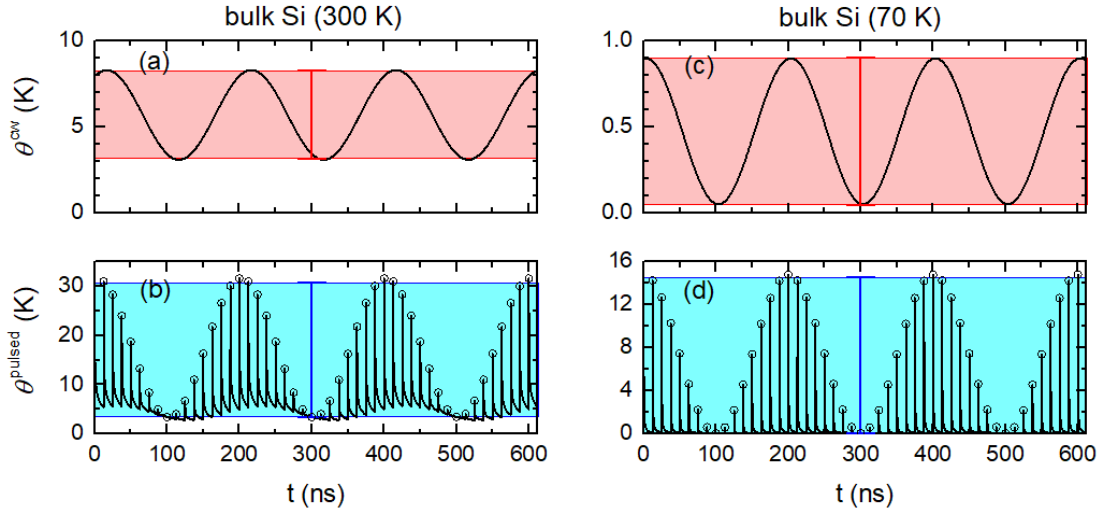


FIG. 4. The time-varying peak temperature rise of a Si substrate heated by a modulated cw laser (a, c) and a modulated pulsed laser (b, d) on the surface at different temperatures of 300 K (a, b) and 70 K (c, d). The averaged heating power is 10 mW and the laser spot size is 5 μm for all the cases. The curves are the numerical results and the shadowed regions represent the estimations using the analytical expressions. The symbols in (b, d) represent the numerical values of the temperature rise evaluated at $t_d = 80$ ps after each pulse.

It would be interesting to compare the temperature rises in Fig. 4 to those in Fig. 1 (1e, 2e). Both temperature rises are evaluated under the same conditions, except that the system for Fig. 1 is 100 nm Al/Si whereas the system for Fig. 4 is a bare Si substrate. Comparison between Fig. 4 and Fig. 1 (1e, 2e) shows that the 100 nm Al layer on top of the Si substrate has little effect on the peak temperature rise of the system at 300 K but would increase the peak temperature rise by ~ 5 times at 70 K. The top layers could thus have different effects on the peak temperature rise of multilayered systems in different situations and should be carefully evaluated to accurately estimate the peak temperature rise of multilayered systems.

4. Effect of top layers on the peak temperature rise in layered structures

The case of multilayered systems is more complicated than the semi-infinite solid mainly because the thin films could act as in-plane heat spreaders, making the heat flux intensity on the surface of the underlying layers different from the original one supplied on the surface of the first layer.

The in-plane heat spreading effect would be larger if the films have a larger $k_r h$, where h is the film thickness. Assuming a linear temperature gradient across the thin films (which could overestimate the temperature rise if the films are too thick to invalidate this assumption), the peak temperature rise of an n -layered system could be estimated as:

$$\theta_{n\text{-layered}} = \left[\frac{2P_0}{\pi w_x w_y} \sum_{i=1}^{n-1} \left(\frac{h_i}{k_{z_i}} + \frac{1}{G_i} \right) + \left(1 + \frac{\sum_{i=1}^{n-1} k_r h_i}{\sqrt{k_r k_{z_n}} \sqrt{w_x w_y}} \right)^{-1} \theta_{\text{sub,dc}} \right] \pm \left[\frac{2P_1}{\pi w_x w_y} \sum_{i=1}^{n-1} \left(\frac{h_i}{k_{z_i}} + \frac{1}{G_i} \right) + \left(1 + \frac{\sum_{i=1}^{n-1} k_r h_i}{\sqrt{k_r k_{z_n}} \sqrt{w_x w_y}} \right)^{-1} \theta_{\text{sub,ac}} \right] \quad (20)$$

where h_i is the thickness of the i -th layer, G_i is the interface thermal conductance between the i -th and the next layers, $\theta_{\text{sub,dc}}$ and $\theta_{\text{sub,ac}}$ are the temperature rise of the semi-infinite substrate evaluated using Eqs. (16, 18, 19).

As a demonstration of Eq. (20), we use this equation to calculate the peak temperature rise of two representative three-layered systems: 1) 100 nm Al/50 nm SiO₂/Si substrate, and 2) 100 nm Ti/200 nm Si/SiO₂ substrate, for both modulated cw and pulsed laser heating. In the first system, the middle layer has a thermal conductivity much lower than the substrate and therefore could incur a significant amount of temperature drop across the film. In the second system, the middle layer has a thermal conductivity much higher than the substrate and therefore should act as an in-plane heat spreader, significantly reducing the heat flux intensity on the surface of the substrate. In the evaluation, the heating power was fixed as $P_0 = P_1 =$

10 mW and the laser spot sizes were fixed as $w_x = 5 \mu\text{m}$ and $w_y = 10 \mu\text{m}$ for both cases. The interface thermal conductance was assumed as $G = 300 \text{ MW/m}^2\text{K}$ for all the interfaces. The thermal conductivities and heat capacities of all the layers used in the calculation are summarized in [Supplementary Information Table S1](#). The estimated temperature rises are compared with the numerical solutions in Fig. 5, where the shadowed regions represent the estimations using the analytical expressions, and the curves are the accurate numerical evaluation of the time-varying peak temperature rises of the systems. The excellent agreement between our estimations and the accurate numerical results proves the validity of our semiempirical correlation Eq. (20). This correlation generally works well but could overestimate the temperature rise when the films are too thick to invalidate the assumption of a linear temperature gradient across the films, for example, in the case of Fig. 5 (a, b).

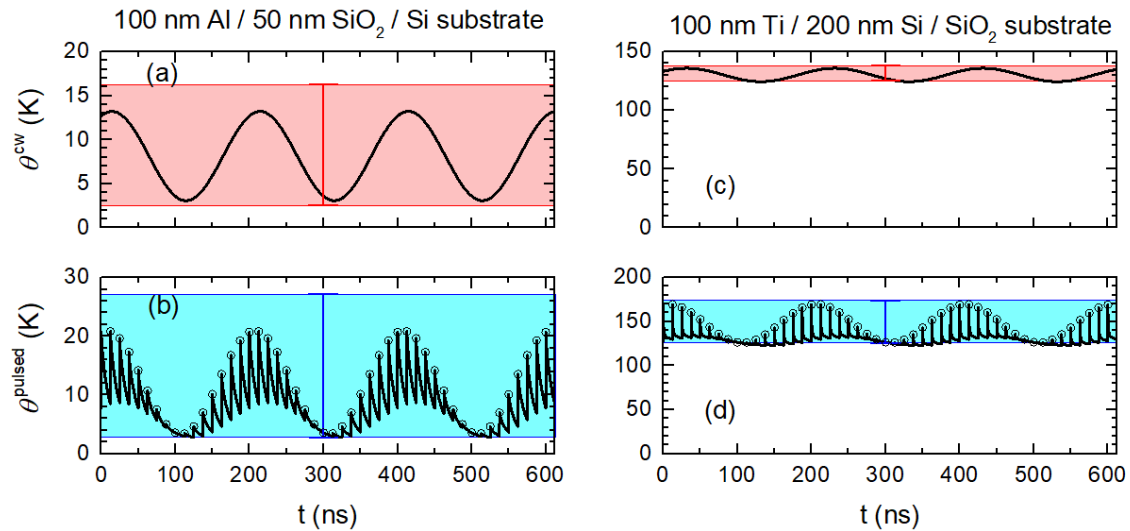


FIG. 5. The time-varying peak temperature rise of a 100 nm Al/50 nm SiO₂/Si substrate (a, b) and a 100 nm Ti/200 nm Si/SiO₂ substrate (c, d) heated by a modulated cw laser (a, c) and a modulated pulsed laser (b, d). The averaged heating power is 10 mW and the laser spot size is $w_x = 5 \mu\text{m}$ and $w_y = 10 \mu\text{m}$ for all the cases. The curves are the accurate numerical results and the shadowed regions represent the estimations using the analytical expressions. The symbols in (b, d) represent the numerical values of the temperature rise evaluated at $t_d = 80$ ps after each pulse.

5. Conclusion

In summary, we provide simple semiempirical correlations for quick and accurate estimation of both the steady-state and transient temperature rise of 3D anisotropic multilayered systems heated by either a cw or a pulsed laser beam. General formalisms of the time-varying temperature rise of 3D anisotropic multilayered systems were first derived for both modulated cw and pulsed laser heating, the evaluation of which, however, requires laborious numerical calculations. We then extract simple semiempirical correlations of the peak temperature rise of semi-infinite solids from the accurate numerical values of several thousand random cases. These correlations were further extended to multilayered systems, taking into account both the temperature drop across the thin films and their in-plane heat spreading effect. These semiempirical correlations have been found to work well within the assumption of a linear temperature gradient across the thin films; otherwise, the temperature rise could be overestimated. These simple semiempirical expressions not only serve the purpose of estimating the maximum temperature rise of 3D anisotropic layered systems in pump-probe thermorefectance experiments and thus greatly benefits these experiments in choosing the appropriate heating power and heater size for the experiments but also enhances our understanding of the physics of temperature rise of multilayered systems under both cw and pulsed laser heating.

Supplementary information

See supplementary material for the derivation of the Green's function, the validation of correlations Eqs. (18, 19), and a table of properties for the cases in Fig. 5.

Acknowledgments

P.J. acknowledges the financial support by the R.K. Mellon Postdoctoral Fellowship.

References:

1. E. Machlin, *Materials Science in Microelectronics I: The Relationships Between Thin Film Processing and Structure*. (Elsevier Science, 2010).

2. F. Bonaccorso, Z. Sun, T. Hasan and A. C. Ferrari, *Nature Photonics* **4** (9), 611-622 (2010).
3. Y. Hamakawa, *Thin-film solar cells: next generation photovoltaics and its applications*. (Springer Science & Business Media, 2013).
4. N. P. Padture, M. Gell and E. H. Jordan, *Science* **296** (5566), 280-284 (2002).
5. M. S. Dresselhaus, G. Chen, M. Y. Tang, R. G. Yang, H. Lee, D. Z. Wang, Z. F. Ren, J. P. Fleurial and P. Gogna, *Adv. Mater.* **19** (8), 1043-1053 (2007).
6. P. Jiang, X. Qian and R. Yang, *J. Appl. Phys.* **124** (16), 161103 (2018).
7. C. Dames, *Annu. Rev. Heat Transfer* **16** (16), 7 (2013).
8. A. T. Ramu and J. E. Bowers, *Rev. Sci. Instrum.* **83** (12), 124903 (2012).
9. J. P. Feser and D. G. Cahill, *Rev. Sci. Instrum.* **83** (10), 104901 (2012).
10. J. P. Feser, J. Liu and D. G. Cahill, *Rev. Sci. Instrum.* **85** (10), 104903 (2014).
11. V. Mishra, C. L. Hardin, J. E. Garay and C. Dames, *Rev. Sci. Instrum.* **86** (5), 054902 (2015).
12. D. Rodin and S. K. Yee, *Rev. Sci. Instrum.* **88** (1), 014902 (2017).
13. P. Jiang, X. Qian and R. Yang, *Rev. Sci. Instrum.* **88** (7), 074901 (2017).
14. P. Jiang, X. Qian and R. Yang, *Rev. Sci. Instrum.* **89** (9), 094902 (2018).
15. P. Jiang, X. Qian, X. Li and R. Yang, *Appl. Phys. Lett.* **113** (23), 232105 (2018).
16. M. Li, J. S. Kang and Y. Hu, *Rev. Sci. Instrum.* **89** (8), 084901 (2018).
17. M. Rahman, M. Shahzadeh, P. Braeuninger-Weimer, S. Hofmann, O. Hellwig and S. Pisana, *J. Appl. Phys.* **123** (24), 245110 (2018).
18. P. Jiang, X. Qian, X. Gu and R. Yang, *Adv. Mater.* **29** (36), 1701068 (2017).
19. X. Qian, P. Jiang and R. Yang, *Materials Today Physics* **3**, 70-75 (2017).
20. P. Jiang, X. Qian, R. Yang and L. Lindsay, *Physical Review Materials* **2** (6), 064005 (2018).
21. X. Qian, P. Jiang, P. Yu, X. Gu, Z. Liu and R. Yang, *Appl. Phys. Lett.* **112** (24), 241901 (2018).
22. D. G. Cahill, P. V. Braun, G. Chen, D. R. Clarke, S. Fan, K. E. Goodson, P. Keblinski, W. P. King, G. D. Mahan, A. Majumdar, H. J. Maris, S. R. Phillpot, E. Pop and L. Shi, *Appl. Phys. Rev.* **1** (1), 011305 (2014).
23. D. G. Cahill, *Rev. Sci. Instrum.* **75** (12), 5119 (2004).
24. J. L. Braun, C. J. Szejewski, A. Giri and P. E. Hopkins, *J. Heat Transfer* **140** (5), 052801 (2018).
25. J. M. Powers, *J. Heat Transfer* **126** (5), 670-675 (2004).
26. A. R. Hadjesfandiari, *International Journal of Materials and Structural Integrity* **8** (4), 209-220 (2014).
27. H. S. Carslaw and J. C. Jaeger, *Conduction of heat in solids*. (Clarendon Press, 1959).

Supplementary Information:

Transient and Steady-State Temperature Rise in Three-Dimensional Anisotropic Layered Structures in Pump-Probe Thermoreflectance Experiments

Puqing Jiang,^{1,2,1)} and Heng Ban^{1,2,2)}

¹*Department of Mechanical Engineering and Materials Science, University of Pittsburgh, Pittsburgh, Pennsylvania 15261, USA*

²*Pittsburgh Quantum Institute, Pittsburgh, Pennsylvania 15260, USA*

Contents:

S1: Deriving the Green's function of 3D anisotropic multilayered systems

S2: Validation of the correlation (Eq. (18)) for $\theta_{dc}^{\text{pulsed}}$

S3: Validation of the correlation (Eq. (19)) for $\theta_{ac}^{\text{pulsed}}$

S4: A table of parameters for the cases in Fig. 5 in the main text

¹ puqing.jiang@pitt.edu

² heng.ban@pitt.edu

S1: Deriving the Green's function of 3D anisotropic multilayered systems

We start from the governing equation of heat diffusion in a 3D anisotropic multilayered system:

$$C \frac{\partial T}{\partial t} = k_x \frac{\partial^2 T}{\partial x^2} + k_y \frac{\partial^2 T}{\partial y^2} + k_z \frac{\partial^2 T}{\partial z^2} + 2k_{xy} \frac{\partial^2 T}{\partial x \partial y} + 2k_{xz} \frac{\partial^2 T}{\partial x \partial z} + 2k_{yz} \frac{\partial^2 T}{\partial y \partial z} \quad (\text{S1-1})$$

This parabolic partial differential equation can be simplified by doing Fourier transforms to in-plane coordinates and time, $T(x, y, z, t) \leftrightarrow \Theta(u, v, z, \omega)$

$$F(u) = \int_{-\infty}^{\infty} f(x) e^{-i2\pi ux} dx$$

$$\mathbb{F} \left\{ \frac{df(x)}{dx} \right\} = i2\pi u F(u)$$

$$\mathbb{F} \left\{ \frac{d^2 f(x)}{dx^2} \right\} = -(2\pi u)^2 F(u)$$

$$(iC\omega)\Theta = -4\pi^2 (k_x u^2 + 2k_{xy} uv + k_y v^2) \Theta + 2i2\pi (k_{xz} u + k_{yz} v) \frac{\partial \Theta}{\partial z} + k_z \frac{\partial^2 \Theta}{\partial z^2} \quad (\text{S1-2})$$

Or more compactly,

$$\frac{\partial^2 \Theta}{\partial z^2} + \lambda_2 \frac{\partial \Theta}{\partial z} - \lambda_1 \Theta = 0 \quad (\text{S1-3})$$

where

$$\lambda_1 \equiv \frac{iC\omega}{k_z} + \frac{4\pi^2 (k_x u^2 + 2k_{xy} uv + k_y v^2)}{k_z} \quad (\text{S1-4})$$

$$\lambda_2 \equiv 2i2\pi \frac{(k_{xz} u + k_{yz} v)}{k_z} \quad (\text{S1-5})$$

The general solution of Eq. (S1-3) is

$$\Theta = e^{u^+ z} B^+ + e^{u^- z} B^- \quad (\text{S1-6})$$

where u^+, u^- are the roots of the equation $x^2 + \lambda_2 x - \lambda_1 = 0$:

$$u^\pm = \frac{-\lambda_2 \pm \sqrt{(\lambda_2)^2 + 4\lambda_1}}{2} \quad (\text{S1-7})$$

and B^+, B^- are the complex numbers to be determined.

The heat flux can be obtained from the temperature Eq. (S1-6) and Fourier's law of heat conduction $Q = -k_z (d\Theta/dz)$ as:

$$Q = -k_z u^+ e^{u^+ z} B^+ - k_z u^- e^{u^- z} B^- \quad (\text{S1-8})$$

It would be convenient to write Eqs. (S1-6) and (S1-8) as matrices as

$$\begin{bmatrix} \Theta \\ Q \end{bmatrix}_{n,z} = [N]_n \begin{bmatrix} B^+ \\ B^- \end{bmatrix}_n \quad (\text{S1-9})$$

$$[N]_n = \begin{bmatrix} 1 & 1 \\ -k_z u^+ & -k_z u^- \end{bmatrix} \begin{bmatrix} e^{u^+ z} & 0 \\ 0 & e^{u^- z} \end{bmatrix}_n \quad (\text{S1-10})$$

where n stands for the n -th layer of the multilayer system, and z is the distance from the surface of the n -th layer.

The constants B^+, B^- for the n -th layer can also be obtained from the surface temperature and heat flux of that layer by setting $z=0$ in Eq. (S1-10) and performing its matrix inversion:

$$\begin{bmatrix} B^+ \\ B^- \end{bmatrix}_n = [M]_n \begin{bmatrix} \Theta \\ Q \end{bmatrix}_{n,z=0} \quad (\text{S1-11})$$

$$[M]_n = \frac{1}{k_z (u^+ - u^-)} \begin{bmatrix} -k_z u^- & -1 \\ k_z u^+ & 1 \end{bmatrix} \quad (\text{S1-12})$$

For heat flow across the interface, an interface conductance G is defined. Therefore, the heat flux across an interface can be written as:

$$Q_{n,z=L} = Q_{n+1,z=0} = G (\Theta_{n,z=L} - \Theta_{n+1,z=0}) \quad (\text{S1-13})$$

From Eq. (S1-13) we also have:

$$\Theta_{n+1,z=0} = \Theta_{n,z=L} - \frac{1}{G} Q_{n,z=L} \quad (\text{S1-14})$$

It is convenient to write Eqs. (S1-13) and (S1-14) as a matrix as

$$\begin{bmatrix} \Theta \\ Q \end{bmatrix}_{n+1,z=0} = [R] \begin{bmatrix} \Theta \\ Q \end{bmatrix}_{n,z=L} \quad (\text{S1-15})$$

$$[R] = \begin{bmatrix} 1 & -1/G \\ 0 & 1 \end{bmatrix} \quad (\text{S1-16})$$

The surface temperature and heat flux can thus be related to those at the bottom of the substrate as

$$\begin{bmatrix} \Theta \\ Q \end{bmatrix}_{n,z=L_n} = [N]_n [M]_n L [R]_1 [N]_1 [M]_1 \begin{bmatrix} \Theta \\ Q \end{bmatrix}_{1,z=0} = \begin{bmatrix} A & B \\ C & D \end{bmatrix} \begin{bmatrix} \Theta \\ Q \end{bmatrix}_{1,z=0} \quad (\text{S1-17})$$

Applying the boundary condition of zero heat flux at the bottom of the semi-infinite substrate yields $0 = C\Theta_{1,z=0} + DQ_{1,z=0}$. The Green's function \hat{G} , which is essentially the surface temperature response due to the applied surface heat flux of unit strength, can thus be solved as

$$\hat{G}(u, \nu) = \frac{\Theta_{1,z=0}}{Q_{1,z=0}} = -\frac{D}{C} \quad (\text{S1-18})$$

With the Green's function \hat{G} determined, the detected temperature response is simply the product of \hat{G} and the heat source function in the frequency domain.

S2: Validation of the correlation (Eq. (18)) for $\theta_{dc}^{\text{pulsed}}$

When a semi-infinite solid is heated by a train of unmodulated laser pulses with an averaged heating power of P_0 , the peak temperature rise $\theta_{dc}^{\text{pulsed}}$ is expressed as the first term of Eq. (17) and could be approximated by the analytical correlation Eq. (18) in the main text, i.e.,

$$\begin{aligned}\theta_{dc}^{\text{pulsed}} &= P_0 \sum_{n=-\infty}^{\infty} \left[e^{-\frac{n^2 \omega_s^2 \tau_p^2}{11.08}} e^{in\omega_s(t-t_0)} \int_{-\infty}^{\infty} \int_{-\infty}^{\infty} \frac{\exp(-\pi^2 u^2 w_x^2 / 2) \exp(-\pi^2 v^2 w_y^2 / 2)}{\sqrt{iC(n\omega_s)k_z + 4\pi^2 k_z (k_x u^2 + k_y v^2)}} dudv \right] \\ &= \theta_{dc, \text{accum}}^{\text{pulsed}} + \theta_{dc, \text{trans}}^{\text{pulsed}} \\ &\approx \xi \frac{P_0}{\sqrt{2\pi w_0^2 k_z k_r}} \left[1 + \left(16 \frac{k_r}{\pi w_0^2 C} \frac{1}{f_{rep}} \right)^{0.18+0.42\xi} \right]^{-1} + \frac{1.1P_0}{f_{rep} \pi w_0^2 \sqrt{k_z C t_d}} \left(1 + \frac{25}{\xi^2} \frac{k_r}{\pi w_0^2 C} t_d \right)^{-1}\end{aligned}\quad (\text{S2-1})$$

To evaluate the validity of Eq. (18), we generate 1000 random cases, with k_x, k_y, k_z independently and randomly varying in the range of 0.5-5000 W/mK, C varying in the range of 0.001-10 MJ/m³K, and w_x, w_y independently and randomly varying in the range of 1-100 μm , as shown in Fig. S1. The tested anisotropy k_z/k_r and α/β have covered a wide range from 10^{-4} to 10^4 , as shown in Fig. S1. For each case, we calculate $\theta_{dc}^{\text{pulsed}}$ as a function of the time t numerically from the first term of Eq. (17), which is considered as an accurate value. We then calculate $\theta_{dc}^{\text{pulsed}}$ for four selected delay time of $t_d = -20, 10, 100, \text{ and } 1000$ ps using the correlation Eq. (18). Note that for $t_d = -20$ ps, $\theta_{dc}^{\text{pulsed}}$ was evaluated by the first term of Eq. (18) only. The deviations between the estimated values and the accurate ones, $\eta = \frac{\theta_{\text{estimate}} - \theta_{\text{numerical}}}{\theta_{\text{numerical}}} \times 100\%$, are plotted as a function of $\xi w_0 \sqrt{C f_{rep} / k_r}$ in Fig. S2.

Figure S2 shows that the correlation Eq. (18) is accurate with an error of $<3\%$ for $t_d = 10$ ps if the dimensionless factor $\xi w_0 \sqrt{C f_{rep} / k_r} > 1$, which could be met in most cases in TDTR experiments. If $\xi w_0 \sqrt{C f_{rep} / k_r} < 1$ or if t_d is too large (e.g., $t_d > 1$ ns) so that the three-

dimensional heat flow dominates, and the simple expression of Eq. (18) would cause a larger error, but still generally less than 50%.

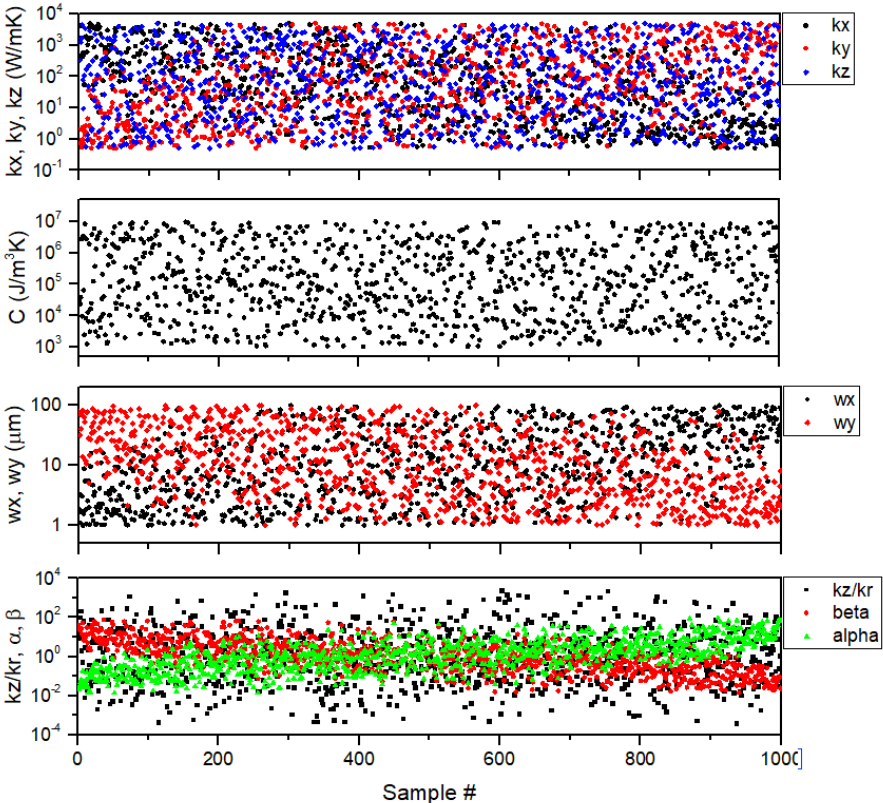


Fig. S1. Parameters of 1000 randomly generated cases for the test of Eq. (18).

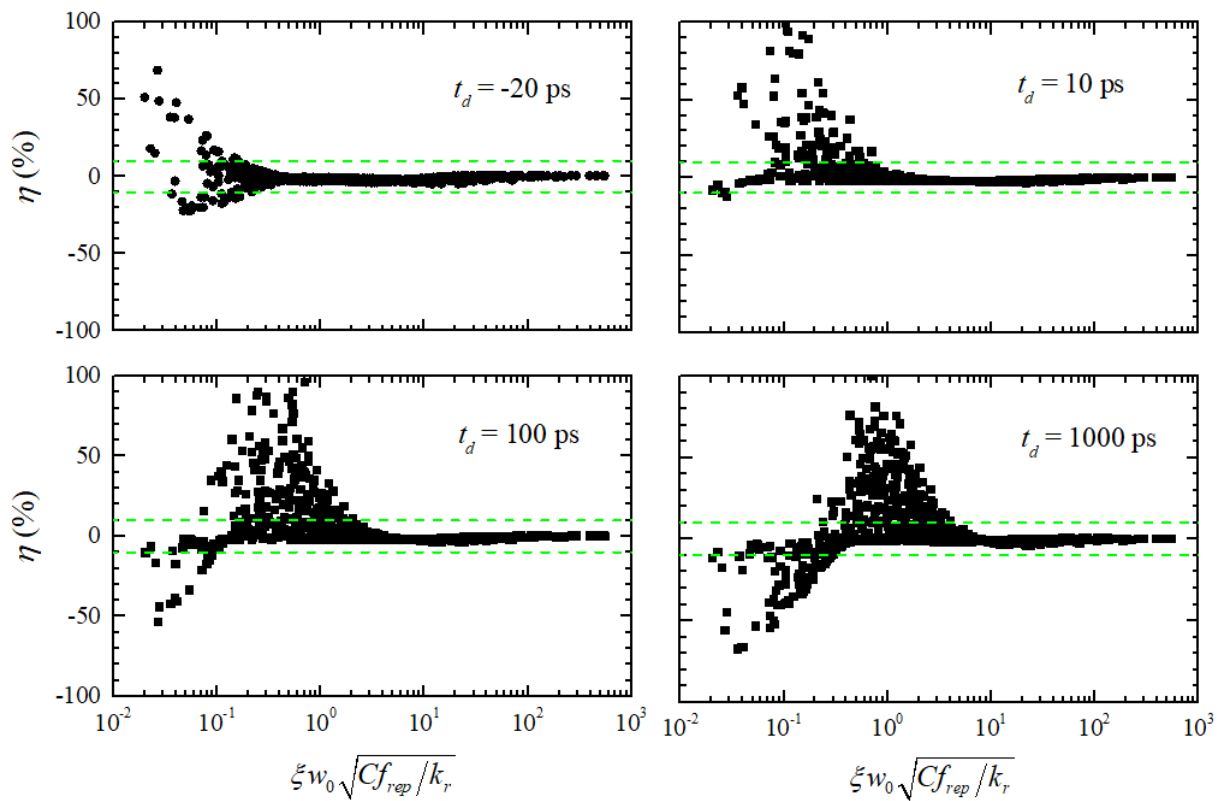


Fig. S2. Deviations of the estimated temperature rise values using Eq. (18) from the accurate numerical values at different delay time of $t_d = -20, 10, 100,$ and 1000 ps.

S3: Validation of the correlations (Eq. (19)) for $\theta_{ac}^{\text{pulsed}}$

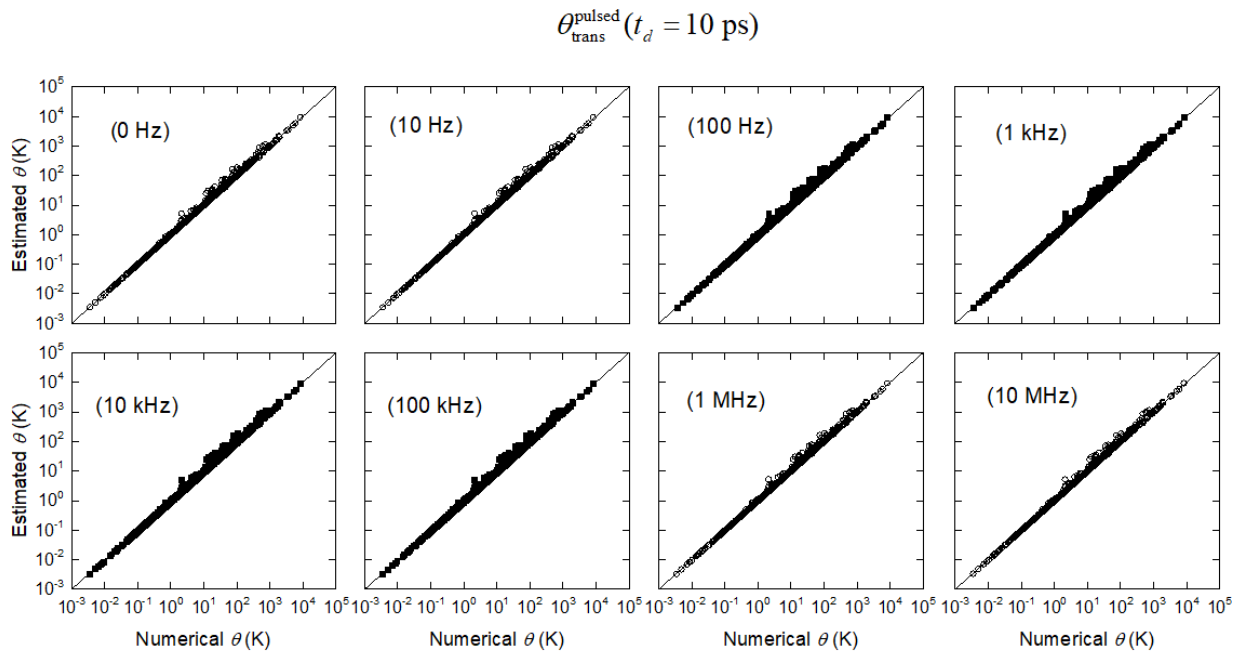
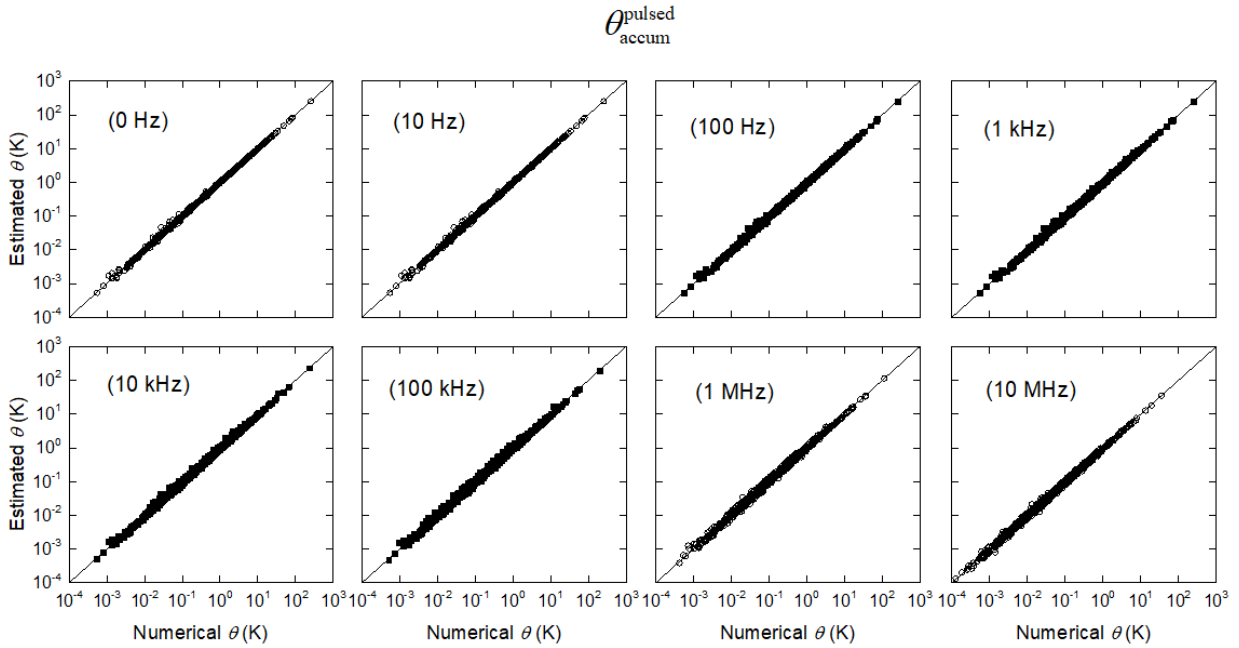
When a semi-infinite solid is heated by a train of sinusoidally modulated laser pulses with the modulation frequency ω_0 and the amplitude of the modulated heating power as P_1 , the peak temperature rise $\theta_{ac}^{\text{pulsed}}$ is expressed as the second term of Eq. (17) and could be approximated by the analytical correlation Eq. (19) in the main text, i.e.,

$$\begin{aligned}
 \theta_{dc}^{\text{pulsed}} &= P_1 \operatorname{Re} \left\{ \sum_{n=-\infty}^{\infty} \left[e^{-\frac{n^2 \omega_s^2 \tau_p^2}{11.08}} e^{in\omega_s(t-t_0)} e^{i\omega_0 t} \int_{-\infty}^{\infty} \int_{-\infty}^{\infty} \frac{\exp(-\pi^2 u^2 w_x^2 / 2) \exp(-\pi^2 v^2 w_y^2 / 2)}{\sqrt{iC(\omega_0 + n\omega_s)k_z + 4\pi^2 k_z (k_x u^2 + k_y v^2)}} dudv \right] \right\} \\
 &= \theta_{ac, \text{accum}}^{\text{pulsed}} + \theta_{ac, \text{trans}}^{\text{pulsed}} \\
 &\approx \frac{P_1}{P_0} \theta_{dc, \text{accum}}^{\text{pulsed}} \left[1 + 4 \left(\frac{w_0}{5} \sqrt{\frac{\omega_0 C}{2\pi k_r}} \right)^{0.36+0.84\xi} \right]^{-1} \left[1 + \pi \sqrt{\frac{\omega_0}{2\pi f_{rep}}} \right]^{-1} \\
 &\quad + \frac{P_1}{P_0} \theta_{dc, \text{trans}}^{\text{pulsed}} \left[1 - \left(1 + \frac{(\omega_0/2\pi)^{-0.11 \log_{10}(4t_d f_{rep})}}{-\log_{10}(4t_d f_{rep})} \right)^{-1} \left(1 + 150 \left(10w_0 \sqrt{\frac{\omega_0 C}{2\pi k_r}} \right)^{-0.6-1.4\xi} \right)^{-1} \right]
 \end{aligned} \tag{S3-1}$$

To evaluate the validity of Eq. (19), we select seven modulation frequencies of 10, 10^2 , ..., and 10^7 Hz. For each frequency, we generate 1000 random cases, with k_x, k_y, k_z independently and randomly varying in the range of 0.5-5000 W/mK, C varying in the range of 0.001-10 MJ/m³K, and w_x, w_y independently and randomly varying in the range of 1-100 μm , similar to the case shown in Fig. S1. For each case, we calculate $\theta_{ac}^{\text{pulsed}}$ as a function of the time t numerically from the second term of Eq. (17), which is considered as an accurate value. We then calculate $\theta_{ac, \text{accum}}^{\text{pulsed}}$ and $\theta_{ac, \text{trans}}^{\text{pulsed}}$ using the correlation Eq. (19). Three delay time of $t_d = 10, 100$, and 1000 ps were chosen to test the correlation of $\theta_{ac, \text{trans}}^{\text{pulsed}}$.

Figure S3 shows the temperature rises $\theta_{ac, \text{accum}}^{\text{pulsed}}$ and $\theta_{ac, \text{trans}}^{\text{pulsed}}$ estimated using correlation Eq. (19), and compared to the accurate numerical values for the 8000 randomly generated cases. Here the heating power was fixed as $P_1 = 1$ mW for all the cases. We can see that the correlation Eq

(19) generally works well. They would have a larger error for large t_d , where the heat flow would become highly three-dimensional and would be too complicated to be evaluated by a simple correlation.



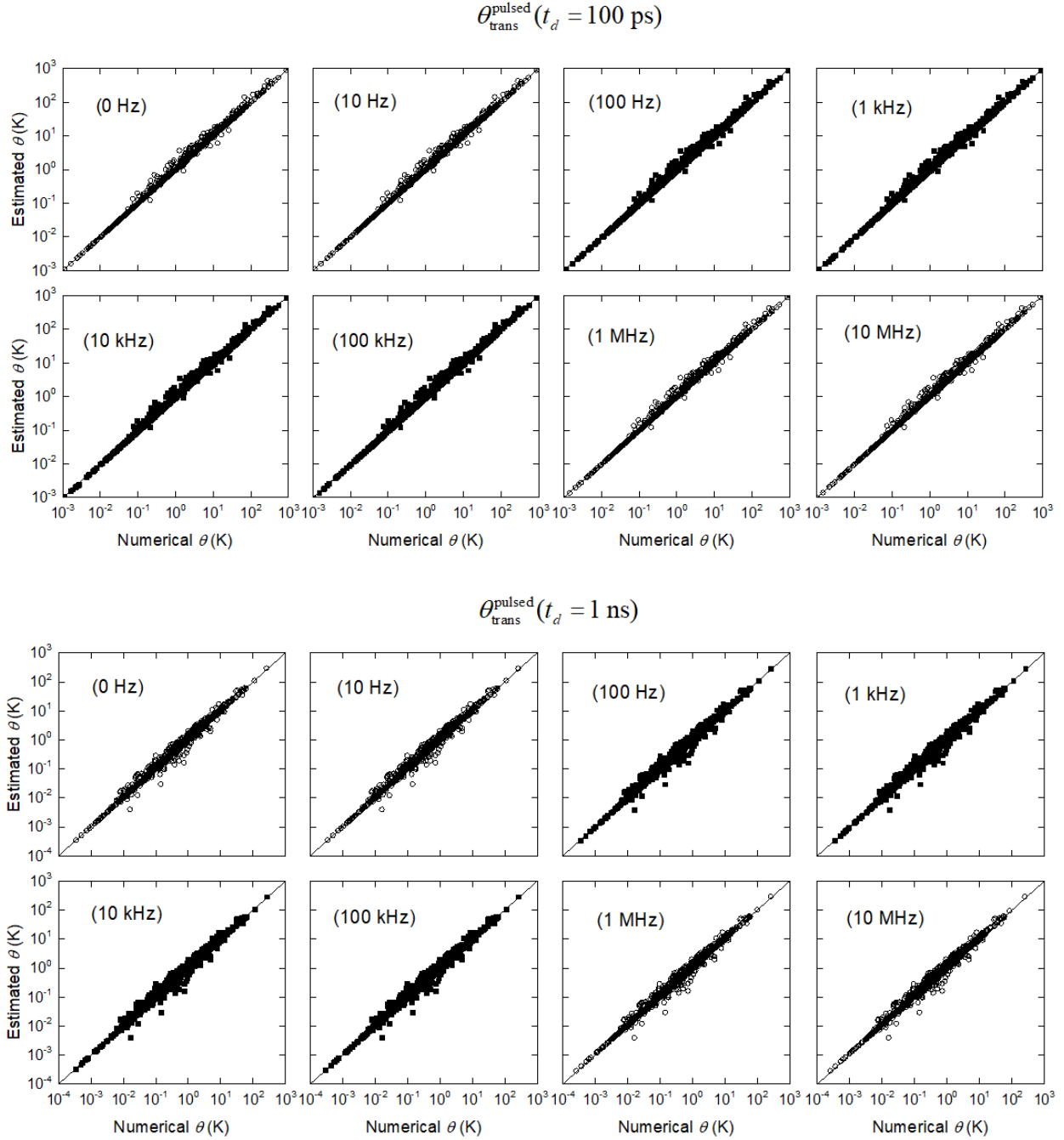


Fig. S3. Estimated temperature rise values using Eq. (19) as compared to the accurate numerical values for modulated pulse heating at different delay time of $t_d = -20, 10, 100,$ and 1000 ps for different modulation frequencies from 10 Hz to 10 MHz.

S4: A table of parameters for the cases in Fig. 5 in the main text

TABLE SI. Parameters of the cases in Fig. 5 in the main text

		Layer 1	Layer 2	Layer 3	
<i>Material</i>	System 1	Al	SiO ₂	Si	
	System 2	Ti	Si	SiO ₂	$w_x = 5 \mu\text{m}$
<i>h (nm)</i>	System 1	100	50	inf	$w_y = 10 \mu\text{m}$
	System 2	100	200	inf	$P_0 = 10 \text{ mW}$
<i>k (W/mK)</i>	System 1	200	1.4	140	$P_1 = 10 \text{ mW}$
	System 2	10	100	1.4	$G = 300 \text{ MW/m}^2\text{K}$
<i>C (MJ/m³K)</i>	System 1	2.4	1.67	1.6	
	System 2	2.35	1.6	1.67	